WATER RESOURCES RESEARCH, VOL. 31, NO. 3, PAGES 699–712, MARCH 1995

Effects of spatial variability and scale on areally averaged evapotranspiration

J. S. Famiglietti
Department of Geological Sciences, University of Texas at Austin

E. F. Wood
Water Resources Program, Department of Civil Engineering and Operations Research, Princeton University
Princeton, New Jersey

Abstract. This paper explores the effects of spatial variability and scale on areally averaged evapotranspiration. A spatially distributed water and energy balance model is employed to determine the effect of explicit patterns of land surface characteristics and atmospheric forcing on areally averaged evapotranspiration over a range of increasing spatial scales. The analysis is performed from the local scale to the catchment scale. The study area is King's Creek catchment, an 11.7 km^2 watershed located on the native tallgrass prairie of Kansas. It is shown that a threshold scale, or representative elementary area (REA) exists for evapotranspiration modeling. It is shown further that the dominant controls on the scaling behavior of catchment-average evapotranspiration, and thus the size of the REA, depend on the dominant controls on its components (bare-soil evaporation, wet canopy evaporation, and dry canopy transpiration) and whether evapotranspiration is occurring at potential rates or soil- and vegetation-controlled rates. The existence of an REA for evapotranspiration modeling suggests that in catchment areas smaller than this threshold scale, actual patterns of model parameters and inputs may be important factors governing catchment-scale evapotranspiration rates in hydrological models. In models applied at scales greater than the REA scale, spatial patterns of dominant process controls can be represented by their statistical distribution functions. It appears that some of our findings are fairly general and will therefore provide a framework for understanding the scaling behavior of areally averaged evapotranspiration at the catchment and larger scales. Our results may have further implications for representing subgrid-scale land surface heterogeneity in hydrological parameterizations for atmospheric models.

Introduction

Large-scale hydrological models are required for a variety of applications in environmental and Earth system studies. Whether these are catchment-, regional-, or global-scale problems, appropriately parameterized models provide a major tool for investigating the behavior and impact of the hydrological cycle within the system of interest. However, owing to its engineering roots, the science of hydrology is currently unable to provide modelers with a theoretical framework for developing larger-scale models. Little guidance is available beyond a researcher's own intuition or assumptions based on a specific application.

For hydrology to advance as a science, *Dooge* [1986] suggests that we must search for laws and unifying concepts with which to expand our scientific knowledge base. In a modeling context, such laws would help to sort out complex issues regarding spatial variability, aggregation, and scaling, which complicate larger-scale modeling problems. How much spatial detail is required as the scale of a hydrologic modeling problem increases? What are the dominant process controls at a particular scale, and how should they be represented within hydrological models? The development of a theoretical framework to address these issues is central to the growth of hydrology as a science.

Paper number 94WR02820.
0043-1397/95/94WR-02820$05.00

Wood et al. [1990] reviewed the first attempts at developing a theoretical understanding of the effects of spatial variability and scale on the quantification and parameterization of storm runoff response. Research on the concept of hydrologic similarity [*Wood and Hebson*, 1986; *Sivapalan et al.*, 1987, 1990] investigated the influence of environmental controls (e.g., topography, soils, climate) on catchment storm response, independent of basin scale. This work showed that consistent scaling parameters could be developed and a scaled storm response model formulated, with the implication that two watersheds with the same set of scaled parameters would exhibit a similar storm response. Such models were employed to investigate both storm responses and flood frequency characteristics. An important outcome of this research was that topographic and soil properties were shown to be dominant controls on runoff generation, so that *Beven*'s [1986] topographic-soil index could be viewed as an index of local hydrologic similarity (i.e., that locations with the same value of the topographic-soil index yield similar storm responses under similar precipitation forcing).

The importance of representing explicit patterns of environmental controls in models of storm runoff response was inves-

tigated by *Wood et al.* [1988] for increasing spatial scales. By averaging storm runoff response over progressively larger subcatchments, they found that the increased sampling of hillslopes leads to a decrease in the difference between subcatchment responses. They found further that a threshold scale exists, above which the variance between storm responses of subcatchments of the same area reaches a minimum. This threshold scale was called a representative elementary area (REA) and was defined as "a critical scale at which implicit continuum assumptions can be used without knowledge of the actual patterns of topographic, soil, or rainfall fields, although it would be necessary to account for the underlying variability of these parameters through distributional functions." For the Coweeta Experimental Basin, *Wood et al.* [1988] demonstrated that the length scale of the REA was 1 km and showed that at scales below this threshold scale, actual patterns of topography, soils, and rainfall had a significant effect on simulated storm response. At scales greater than the REA, they showed that spatial variability in dominant topographic and soil properties could be represented using a statistical distribution function rather than explicit patterns, greatly simplifying the runoff modeling problem without significant biases resulting in computed storm response. The concept of an REA for storm response modeling offers a framework for simultaneously addressing problems of spatial variability and spatial scale. As such, it may develop into a fundamental building block for storm response modeling, as evidenced by continuing research on this problem [*Bloschl et al.*, 1995a, b; *Woods and Sivapalan*, 1995].

The purpose of this paper is to explore whether similar concepts of local hydrologic similarity and of a threshold (REA) scale apply to interstorm processes and hence whether a threshold (REA) scale exists for catchment-scale evapotranspiration modeling. Since an REA has been shown to exist for storm response modeling, the existence of an REA for interstorm modeling implies that the problem of continuous simulation of storm runoff and interstorm energy balance partitioning can be greatly simplified at the catchment scale. Actual patterns of important land surface variables could be replaced by their distribution functions in catchment-scale water and energy balance models if the watershed area exceeds the REA.

The existence of an REA for both runoff and evapotranspiration modeling may also have implications at the larger grid scales of mesoscale and global atmospheric models. Since the length scale of the REA, at least for storm response modeling, is much less than the length scale of atmospheric model grid cells (O(10 km) for mesoscale models and O(100 km) for global models), the existence of such a threshold scale offers encouragement that important subgrid-scale hydrological heterogeneity can be represented fairly easily in land surface parameterizations for atmospheric models. (Here, $O(\ )$ implies a length scale with an order of magnitude shown in parentheses.) This point will be discussed further later in this paper.

In the remainder of this paper we address the following questions. First, does an REA exist for catchment-scale evapotranspiration modeling and what are the process controls that dictate its existence and length scale? Second, what are its implications for hydrologic modeling, and relatedly, do concepts of local hydrologic similarity hold at the catchment scale for interstorm modeling? A series of numerical experiments were performed to address the first question. These experiments and their results are described below. Regarding the second question, insights into the modeling implications are addressed in the discussion section. Finally, the salient features of this work are summarized in a concluding section.

Before describing the details of this study, a review of the various spatial scales, as interpreted in this work, is in order. The term local scale refers to the point scale, or the area immediately surrounding a field instrument. In this paper, that definition is extended to the length scale of the smallest computational unit employed in this work (30 m). The catchment scale refers to watershed areas smaller than the grid scale of mesoscale atmospheric models, defined above. The term macroscale is defined more loosely as the grid scale of either mesoscale or global atmospheric models. The regional scale refers to much larger land surface areas covering millions of square kilometers (length scales greater than O(1000 km)).

Methods

Central to investigating the existence of an REA is understanding the role of explicit spatial patterns in producing catchment-averaged hydrologic response as catchment scale increases. In this work, increasing spatial scale is represented by progressively larger subcatchments within the catchment of interest. We expect that at small scales, actual patterns of model parameters and inputs (e.g., root zone moisture content, soil properties, vegetation, solar radiation) are important factors governing catchment-scale evapotranspiration rates, where the term evapotranspiration is used in the traditional sense to represent the sum of bare-soil evaporation, dry canopy transpiration, and evaporation from the wet canopy. However, as catchment scale increases, more of the variability in the distributions underlying these patterns is sampled. We suspect that with increasing spatial scale, a threshold scale is exceeded, beyond which the variance in catchment-averaged evapotranspiration rates reaches a minimum for subcatchments of the same size. At scales larger than the threshold, or REA scale, the mean evapotranspiration rate may no longer depend on the actual patterns of variability, but rather on the statistical characteristics representing the underlying distributions. A procedure for investigating the existence of an REA for evapotranspiration modeling and interstorm process controls is described below. The implications of these findings are addressed in the discussion section.

Owing to the lack of high-resolution, spatially detailed water and energy balance data sets, we adopt a simulation-based approach. The requirements for this type of simulation experiment are outlined by *Wood et al.* [1988]. First, a disaggregation scheme must exist for the study catchment so that it can be partitioned into a number of smaller subcatchments. Second, a local model of hydrologic processes must exist whose scale of application is much smaller than the smallest subcatchment, so that the average response of any subcatchment is equivalent to the average of the local responses within it. Third, spatially distributed model inputs and parameters must exist so that the model can represent spatial patterns within the study catchment.

The study catchment is the King's Creek catchment, an 11.7 km^2 watershed located on the native tallgrass prairie near Manhattan, Kansas. This region was the site of the First International Satellite Land Surface Climatology Project (ISLSCP) Field Experiment (FIFE) during the summers of 1987 and 1989 [*Sellers et al.*, 1992]. The King's Creek catchment is located in the northwest quadrant of the 15 km $\times$ 15 km FIFE site. A 30-m U.S. Geological Survey digital elevation model

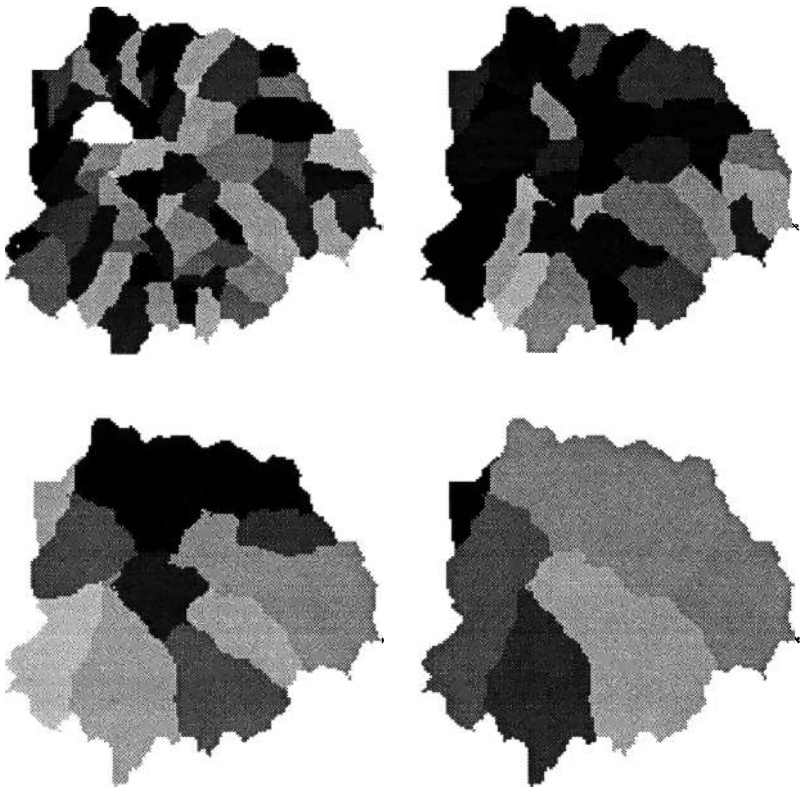

Figure 1. Disaggregation of the King's Creek catchment into subcatchments. From left to right and top to bottom: 66, 39, 13, and 5 subcatchments. North is at top of page. Catchment area is 11.7 km^2.

(DEM) is available for the King's Creek catchment. Topographic analysis of the DEM yielded the four levels of discretization shown in Figure 1. The first level of disaggregation partitions the catchment into 66 subcatchments. The second level yields 39 subcatchments, the third 13, and the fourth 5 subcatchments. Thus the first requirement (partitioning into subcatchments) is satisfied by the FIFE data.

The second requirement (a local model of hydrological processes) is satisfied by the spatially distributed water and energy balance model described in detail by *Famiglietti and Wood* [1994a]. This model is essentially a local water and energy balance model applied at each grid element of a discretized catchment, with model grids coupled together through lateral subsurface flow processes. A brief description of the model is given in the appendix.

Famiglietti and Wood [1994b] demonstrated that the third requirement (spatially distributed model inputs and parameters) is also satisfied by the FIFE data set, which is archived at NASA Goddard Space Flight Center in the FIFE information system (FIS). In that work, the King's Creek catchment topography was represented by the local 30-m DEM. The topographic-soil index required for the model was determined for each grid element in the catchment using the FIFE DEM and soil data obtained from the FIS. Spatial patterns of precipitation and other soil parameters were also obtained from the FIS. The spatially distributed model was shown to reproduce observed mean evapotranspiration rates well. Modeled patterns of evapotranspiration rates were consistent with those obtained independently by other FIFE researchers using a combination of remote- and ground-based observations [*Holwill and Stewart*, 1992; *Jedlovec and Atkinson*, 1992].

Although the model is well suited to represent spatial patterns of all model parameters and inputs, in actuality, the King's Creek catchment has little variability in soil properties (predominantly silty clay loam), vegetation (predominantly native tallgrass), and topography (roughly 100 m of elevation difference). However, *Schimel et al.* [1991] noted that topographic redistribution of soil water results in significant downslope differences in moisture availability at FIFE, and ground-based and remotely sensed observations of surface soil moisture by *Schmugge et al.* [1988] showed clear evidence of topographic gradients in surface wetness. Consequently, we expect spatial variability in root zone moisture content to be an important control on areally averaged evapotranspiration rates, particularly during periods of moisture stress, when evapotranspiration frequently occurs at soil- or vegetation-controlled rates (known as exfiltration and transpiration capacities, or the maximum rates at which soil and vegetation can supply moisture to the soil or canopy surface, respectively). Figure 2 shows the general form of the transpiration capacity-moisture content and exfiltration capacity-moisture content relationships used in the spatially distributed model. These relationships suggest that when soil and vegetation controls of evapotranspiration are active, and the spatial distribution of root zone moisture content includes the nonlinear portions of the curves, evapotranspiration will not scale up at King's Creek. (The term "scaling up" is defined here as an insignificant bias between evapotranspiration computed with spatially variable versus spatially constant, or "effective" model parameters and inputs.) In this study, we explore this hypothesis by conducting our evapotranspiration simulations during the fourth FIFE intensive field campaign (IFC4) (October 5–16,

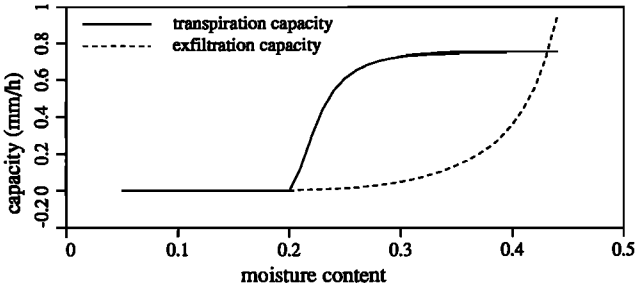

Figure 2. General form of transpiration capacity and exfiltration capacity versus moisture content utilized by *Famiglietti and Wood* [1994a].

1987), a period during which soil and vegetation controls of evapotranspiration were active. The spatial distribution of initial root zone moisture content shown in Plate 2 of *Famiglietti and Wood* [1994b] was also employed in the simulations. This pattern of moisture content includes wetter regions along stream channels and drier regions upslope. Consequently, these initial moisture conditions yield significant spatial variability in transpiration and exfiltration capacities, so that the nonlinearity shown in Figure 2 is well represented within the catchment.

The spatially distributed model was applied at the King's Creek catchment for the first five (rain-free) days of IFC4 (October 5–9, 1987). Spatial patterns and values of all model parameters and inputs are given by *Famiglietti and Wood* [1994b] with the following differences. Some allowance for spatially variable vegetation parameters was made in this study that was not made previously. A 5-m-tall vegetation was modeled along the stream channels (roughly 5% of the catchment surface area). In these locations, the measurement height z_a was set equal to 7 m, the roughness length z_0 was assumed equal to 0.8 m, the zero plane displacement d was assumed equal to 3.35 m, and a value of 5×10^9 s/m was assumed for R_u, the root resistance. The remainder of the catchment was assumed covered with 0.34-m-tall native prairie grass. Spatially distributed clear-sky solar radiation was also employed in this study and was provided by R. Dubayah (personal communication, 1992) for the FIFE site for October 5, 1987. Since this is primarily a sensitivity study and not a validation study, the solar radiation data of October 5 were also used to force model simulations of October 6–9. This simulation, in which all available spatial patterns of model parameters and inputs were utilized, will be referred to as the control run in future sections. Additional simulations were run in which these spatially distributed data were systematically held at catchment-average values. These simulations will be referred to as the sensitivity runs.

For a particular simulation, the local (grid element) evapotranspiration fluxes were averaged over the various subcatchments shown in Figure 1 at selected times during the run. The average evapotranspiration rates for each of the subcatchments were sorted by subcatchment area. Average evapotranspiration rates were then plotted versus subcatchment area to analyze the effect of spatial variability on catchment-average evapotranspiration with increasing spatial scale. To determine the sensitivity of catchment-average evapotranspiration to spatial variability in the various model parameters and inputs, plots of catchment-average evapotranspiration rate versus catchment area were compared for the control and sensitivity runs at different times during the simulations. Thus the primary purpose of the control run was to establish the existence of an REA for evapotranspiration modeling, while the sensitivity runs were designed to provide insight into the processes that dictate its existence and length scale.

Results

Figure 3 shows simulated catchment-average evapotranspiration for the control run. To analyze the effect of spatial variability and scale on catchment-average evapotranspiration, the procedure outlined in the preceding paragraph was applied at numerous times during the simulation. The results for three times, 1245, 1415, and 1815 UT, October 7, 1987 (0745, 0915, and 1315 LT; times 56, 57.5, and 61.5 in Figure 3), are shown in Figure 4a. For comparison, Figure 4b shows catchment-average evapotranspiration versus catchment area for a sensitivity run in which all model parameters and inputs were held at catchment-average values. Figure 4 clearly shows a number of effects on areally averaged evapotranspiration resulting from the combined impact of spatial variability and increasing spatial scale. First, Figure 4a shows that the effect of spatial variability has been, in general, to increase the variability in the catchment-average evapotranspiration rate at small scales and to increase the mean rate at all scales. The difference in mean rates across scales between Figures 4a and 4b is indicative of significant nonlinearities that cannot be captured with catchment-averaged parameter values and model inputs. This point will be discussed further in later sections. Second, Figure 4a suggests that a threshold (REA) scale does in fact exist that marks the transition from highly variable mean behavior at small scales, to stable mean behavior at larger scales. It is inferred that for areas larger than the REA, most of the variability in model parameters and inputs has been sampled, so that at larger scales, the mean evapotranspiration rate stabilizes. Finally, this figure shows that the variability in the mean

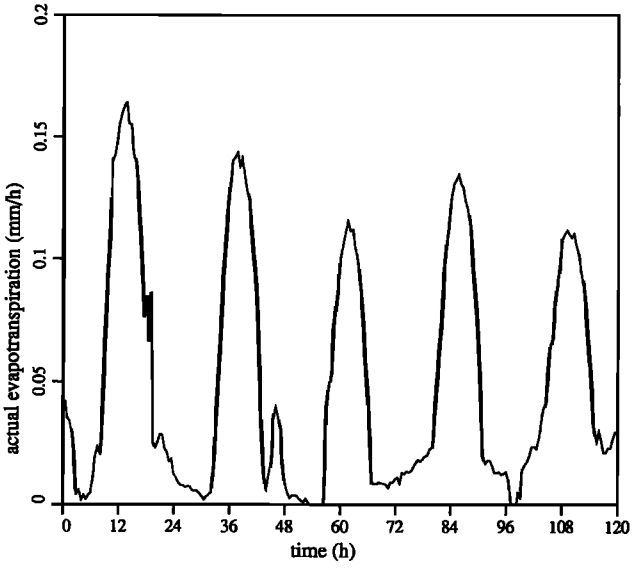

Figure 3. Evapotranspiration computed for the King's Creek catchment during FIFE IFC4, October 5–9, 1987 (control run). Time 0 corresponds to 0445 UT, October 5. Simulation time step is 0.5 hours.

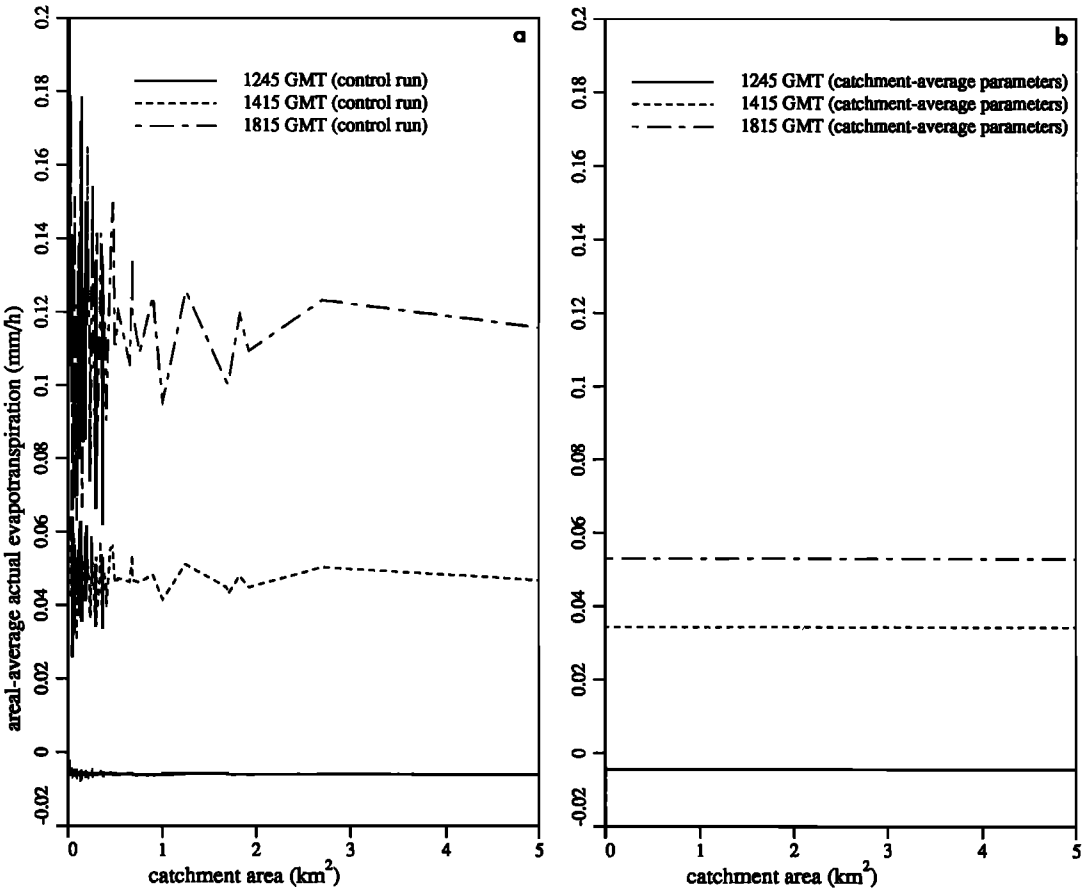

Figure 4. Computed catchment-average evapotranspiration rate versus catchment area for 1245, 1415, and 1815 UT, October 7, 1987: (a) control run and (b) all parameters spatially averaged.

evapotranspiration rate at small scales, and thus the REA scale, is greater at midday than in the morning.

Note that the times shown in Figure 4 should be considered representative times for the simulation. Similar scaling behavior was observed throughout the simulation at the corresponding times each day (i.e., an increase in the REA scale from local scales in the morning to 1–2 km^2 at midday, and decreasing back to local scales in the late afternoon). The term "scaling behavior" is defined here as the relationship between areally averaged evapotranspiration rate and spatial scale shown in Figure 4.

The significant bias between evapotranspiration computed with and without spatially variable model parameters indicates that spatial heterogeneity in land surface-atmosphere interaction plays a major role in the simulation of catchment-average evapotranspiration. To elucidate fundamental relationships between spatial variability, scale, and evapotranspiration fluxes, we investigated the scaling behavior of the three components of simulated evapotranspiration individually (evaporation from the wet canopy, transpiration from the dry canopy, and evaporation from bare soils) at the same times as in Figure 4. In each case an attempt was made to determine the spatial patterns of model parameters to which the component was most sensitive, and whether this sensitivity changed diurnally. This analysis should result in a better understanding of the important process controls on areally averaged evapotranspiration, and thus the scaling behavior shown in Figure 4a, with implications for how these controls should be represented within land surface parameterizations.

Results of the scaling behavior analysis are described in detail for bare soil evaporation, since evaporation from bare soils was the primary component of evapotranspiration during FIFE IFC4 due to senescence of the native tallgrass (see Figure 5). The results for wet canopy evaporation and dry canopy transpiration are analogous to those for bare-soil evaporation. These results are presented in detail by *Famiglietti* [1992] and are only briefly described here.

Bare-Soil Evaporation

The actual rate of evaporation from bare soil, e_{bs}, is given by *Famiglietti and Wood* [1994a] as

$$e_{bs}(i) = \min [e^*(i), e_{pe}(i)] \quad (1)$$

where i is the grid element index, e^* is the local exfiltration capacity, and e_{pe} is the local potential evaporation rate. The exfiltration capacity is a function of soil moisture content at the start of an interstorm period, the properties of the soil, and the cumulative evaporation at i since the start of the interstorm period. The potential evaporation rate is defined as the evaporation rate when soil moisture content is not limiting. It is therefore a function of current atmospheric conditions and soil properties which affect the roughness and thermal properties of the soil. When the exfiltration capacity is less than the

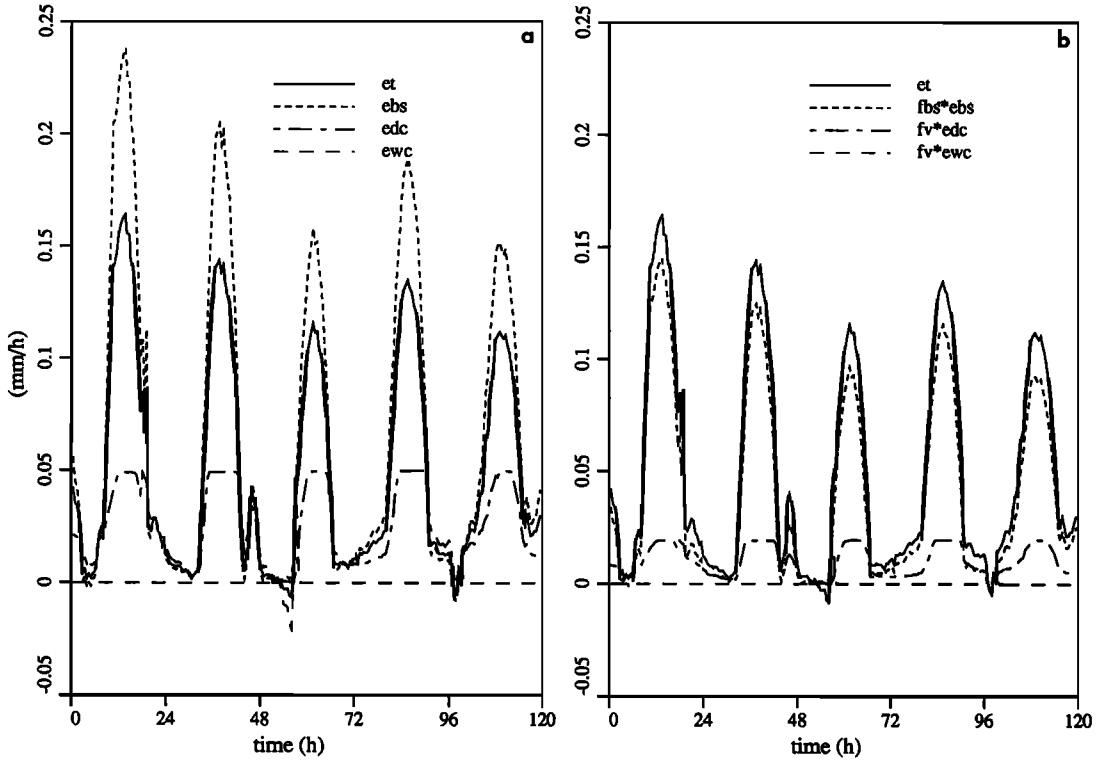

Figure 5. Evapotranspiration computed for the King's Creek catchment during FIFE IFC4, October 5–9, 1987 (control run) (a) for bare soil (ebs), dry canopy (edc), and wet canopy (ewc) components, and total evapotranspiration (et); (b) for each component weighted by the fraction of bare soil (fbs) or the fraction of vegetated surface (fv). Time 0 corresponds to 0445 UT, October 5.

potential evaporation rate, the actual evaporation rate is equal to the exfiltration capacity, i.e., the bare-soil evaporation rate is limited by the soil column's ability to conduct water to the land surface. Evaporation under these conditions is known as soil-controlled evaporation. In this section the scaling behavior of the exfiltration capacity and the potential evaporation is investigated, as is their combined impact on actual bare-soil evaporation.

Potential evaporation. Figure 6 shows the computed catchment-average potential evaporation rate versus catchment scale for the three representative time steps during the control simulation (1245, 1415, and 1815 UT, October 7, 1987). In each case, the catchment-average potential evaporation shows more variability at small scales than at large scales. Figure 6 suggests that a threshold (REA) scale exists that marks this transition in mean behavior. This figure also shows that the variability in catchment-average potential evaporation at small scales, and thus the REA scale, is greater at midday than in the morning.

To better understand the sources of variation in computed catchment-average potential evaporation with scale, two sensitivity runs were simulated. Of the parameters assumed spatially variable in this paper, those that affect potential evaporation most significantly are solar radiation and soil properties. The two sensitivity runs used the following combinations of model inputs: spatially constant solar radiation and spatially constant soil properties (crcs); and spatially constant solar radiation and spatially variable soil properties (crvs). These were compared with the control run, which was generated with spatially variable solar radiation data and spatially variable soil properties (vrvs). Spatially constant model inputs were held at their catchment-average values.

Figure 7 shows computed catchment-average potential evaporation rates versus catchment scale at 1815 UT for the control and sensitivity runs. The solid line represents catchment-average potential evaporation for the case of spatially constant solar radiation and soil properties. The inclusion of spatially variable soil properties has a minor effect on catchment-average potential evaporation rates at all scales, probably owing to similarities in soil types within the catchment. The inclusion of spatially variable solar radiation has a significant impact on the catchment-average potential evaporation, yielding a high degree of variability at small scales. At larger scales, however, spatial variability in solar radiation has less of an effect on catchment-average potential evaporation rates. The variability in solar radiation within the catchment is not great enough (i.e., topographic variability is not great enough) to yield strong nonlinearities in potential evaporation rates so that it scales up reasonably well at larger spatial areas. Figure 7 also shows that the REA scale for the potential evaporation rate at this time is 1.0–2.0 km^2. We believe that at this scale, most of the spatial variability in the solar radiation has been sampled, so that at larger scales the mean potential evaporation rate stabilizes. The increase in the REA scale with time toward midday, mentioned above, is due to the corresponding increase in variability in solar radiation within the catchment.

Exfiltration capacity. To better understand the scaling behavior of catchment-average exfiltration capacity, three sensitivity runs were simulated and compared with the control run (vmvrvs). Of the parameters that are assumed spatially variable

in this work, those with the most significant impact on exfiltration capacities include root zone moisture content, soil properties, and solar radiation (through its impact on cumulative evaporation, of which exfiltration capacity is a function). We systematically held these parameters at their catchment-average values in the sensitivity runs. In the first simulation, spatially constant soil moisture, solar radiation, and soil properties were employed (cmcrcs). The second simulation maintained constant solar radiation and soil properties but was initialized with the spatial distribution of root zone moisture content shown in Plate 2 of *Famiglietti and Wood* [1994b] (vmcrcs). The third simulation added spatially variable soil properties to the list of model inputs used in the second simulation (vmcrvs).

Figure 8 shows catchment-average exfiltration capacity versus catchment scale at 1815 UT, October 7, 1987, for the control and sensitivity runs described above. The lower line (cmcrcs) represents catchment-average exfiltration capacity for spatially constant soil moisture, solar radiation, and soil properties. The upper line (vmcrcs) shows the impact of including spatially variable moisture content in the simulation. The mean exfiltration capacity has increased over all scales, and its variability has increased significantly at small scales. The inclusion of spatially variable soil properties has lowered the mean exfiltration capacity over all scales. The inclusion of spatially variable solar radiation has little impact on the mean exfiltration capacity over all scales. Figure 8 implies that, for the parameter combinations tested, the dominant control on the scaling behavior of the catchment-average exfiltration capacity is the spatial distribution of moisture content. Figure 8 also shows that the REA scale for exfiltration capacity is roughly 1.0–2.0 km^2. At this scale, most of the spatial variability in the moisture content, solar radiation, and soil properties has been sampled, so that at larger scales the mean exfiltration capacity stabilizes.

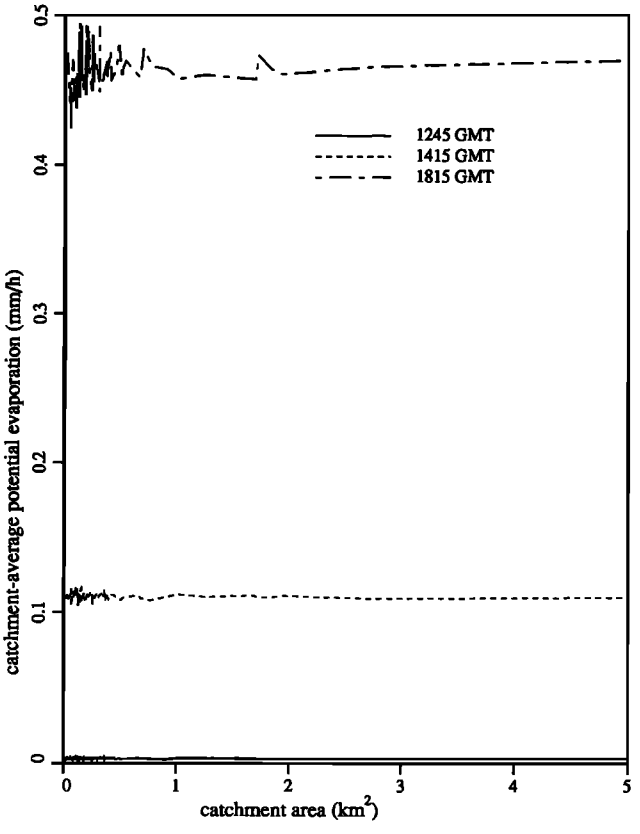

Figure 6. Computed catchment-average potential evaporation versus catchment area at three times: 1245, 1415, and 1815 UT, October 7, 1987.

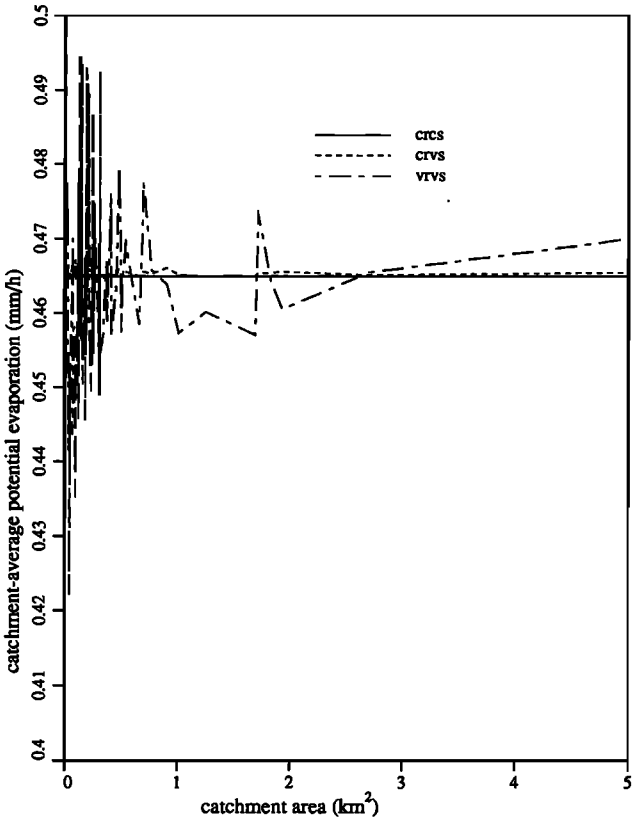

Figure 7. Computed catchment-average potential evaporation versus catchment area at 1815 UT, October 7, 1987, for spatially constant solar radiation and spatially constant soil properties (crcs); spatially constant solar radiation and spatially variable soil properties (crvs); and spatially variable solar radiation and spatially variable soil properties (vrvs).

These results are best understood by considering the relationship of the spatial distribution of root zone moisture content to the exfiltration capacity–soil moisture relationship shown in Figure 2. When the moisture content distribution lies on a linear portion of this curve, spatial variability in moisture content has little effect on the catchment-average exfiltration capacity. In this range of the soil moisture content distribution, exfiltration capacities scale linearly so that the effect of variable moisture content is the same as that found using catchment-averaged soil moisture values. However, when the moisture content distribution includes the nonlinear portion of the curve, as in this case, spatial variability in moisture content has a significant impact on the catchment-average exfiltration capacity because linear averaging will not equal the effective-parameter-based exfiltration capacity.

Figure 8 shows that the impact of including variable soil properties is much less significant than that of variable soil moisture. As mentioned above, its effect has been to lower the catchment-average exfiltration capacity over all scales, since the simulations run with spatially averaged soil parameters resulted in higher root zone moisture contents (and thus exfil-

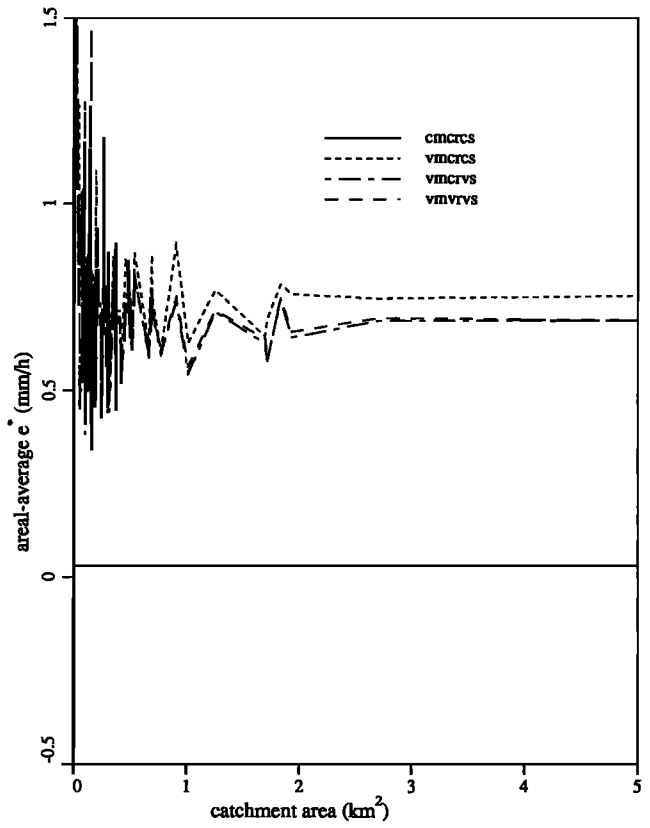

Figure 8. Computed catchment-average exfiltration capacity versus catchment area at 1815 UT, October 7, 1987, for the following combinations of model inputs: spatially constant moisture content, solar radiation, and soil properties (cmcrcs); spatially variable moisture content and spatially constant solar radiation and soil properties (vmcrcs); spatially variable soil moisture and soil properties and spatially constant solar radiation (vmcrvs); spatially variable moisture content, solar radiation and soil properties (vmvrvs).

tration capacities) than the variable soil parameter case. The minimal impact is likely a result of the lack of variability in soil types over the catchment, so that any nonlinearities in exfiltration capacity resulting from differences in soil properties are not well represented within King's Creek. Variability in solar radiation has minimal impact on the results, as it is only weakly related to exfiltration capacity through its impact on potential evaporation rates and thus cumulative evaporation.

Actual bare-soil evaporation. The effect of including spatial patterns of soil moisture and other model inputs in a spatially distributed catchment simulation is that different catchment locations evaporate at different rates simultaneously. At any time, all bare-soil locations within the catchment fall into two groups: those evaporating at the potential rate and those evaporating at soil-controlled exfiltration capacities. Thus variability in the catchment-average actual evaporation rate with scale is a function of the relative amounts of land surface evaporating at potential or soil-controlled rates and the scaling behavior of these two components. (See *Famiglietti and Wood* [1994a], who compute the amount of land surface evaporating at potential or soil-controlled rates for each time step during IFC4.) If the REA scale differs for the potential and soil-controlled components of evaporation, then the REA scale for the actual evaporation rate should vary according to the amount of land surface evaporating under either condition. To explore these interactions, actual bare-soil evaporation was computed for the first five days of IFC4 for the control run. The catchment-average potential evaporation rate, soil-controlled exfiltration capacity, and actual evaporation rate were plotted in Figure 9 versus catchment scale for 1245, 1415, and 1815 UT, October 7, 1987.

Figure 9a shows the results at 1245 UT. In the early morning, the potential evaporation rate is low, as shown by the lower line, and the simulation results indicate that most of the catchment evaporates at this low rate. The catchment-average actual evaporation rate should nearly equal the catchment-average rate of potential evaporation. Figure 9a shows that in fact the two are essentially equal. In the morning, when most of the catchment is evaporating at the potential rate, the dominant controls on the scaling behavior of the catchment-average actual evaporation rate (and thus its REA) are those associated with the potential evaporation rate.

Figure 9b presents the results for 1415 UT (midmorning). As the potential evaporation rate increases (solid line), more of the catchment evaporates at soil-controlled rates. Thus the degree of variability in the catchment-average actual evaporation (dot-dashed line) at small scales is greater than that of the potential evaporation, but less than that of the exfiltration capacity. Both the potential evaporation and exfiltration capacity components are contributing to the variability in catchment-average actual evaporation at small scales, and to the mean actual evaporation rate over all scales.

The results for 1815 UT (midday) are displayed in Figure 9c. At midday the potential evaporation rate (solid line) exceeds the exfiltration capacity (short-dashed line) over much of the catchment. Thus the catchment-average actual evaporation rate reflects more of the variability of the catchment-average exfiltration capacity. More bare-soil locations within the catchment have switched from evaporation at potential rates to soil-controlled rates. Consequently, the dominant controls of the scaling behavior of catchment-average actual evaporation have switched from those associated with the potential evaporation rate to those associated with the exfiltration capacity.

Some readers may find Figure 9c confusing, since the average exfiltration capacity appears to exceed the average potential evaporation rate over all scales, even though we have stated that by midday, most catchment locations evaporate at soil-controlled rates. The reason that the scaling behavior of the exfiltration capacity plots above that of the potential rate is again due to its nonlinear relationship to soil moisture. Most of the catchment is relatively dry with low exfiltration capacities. However, wetter locations, such as those along the stream network, have very high exfiltration capacities which drive the catchment-average exfiltration capacity above the catchment-average potential evaporation rate.

Figure 10 shows the catchment-average actual evaporation rate versus catchment scale for 1245, 1415, and 1815 UT. This figure clearly shows the increase in variability of the catchment-average actual evaporation rate at small scales with time. Figure 10 also suggests that the REA scale increases with time, from very small scales in the morning, to 1.0–2.0 km^2 at midday. Both the increased variability at small scales and the increase in the REA scale reflect the change in evaporation modes within the catchment, from predominantly potential rates in the morning, to predominantly soil-controlled rates at midday.

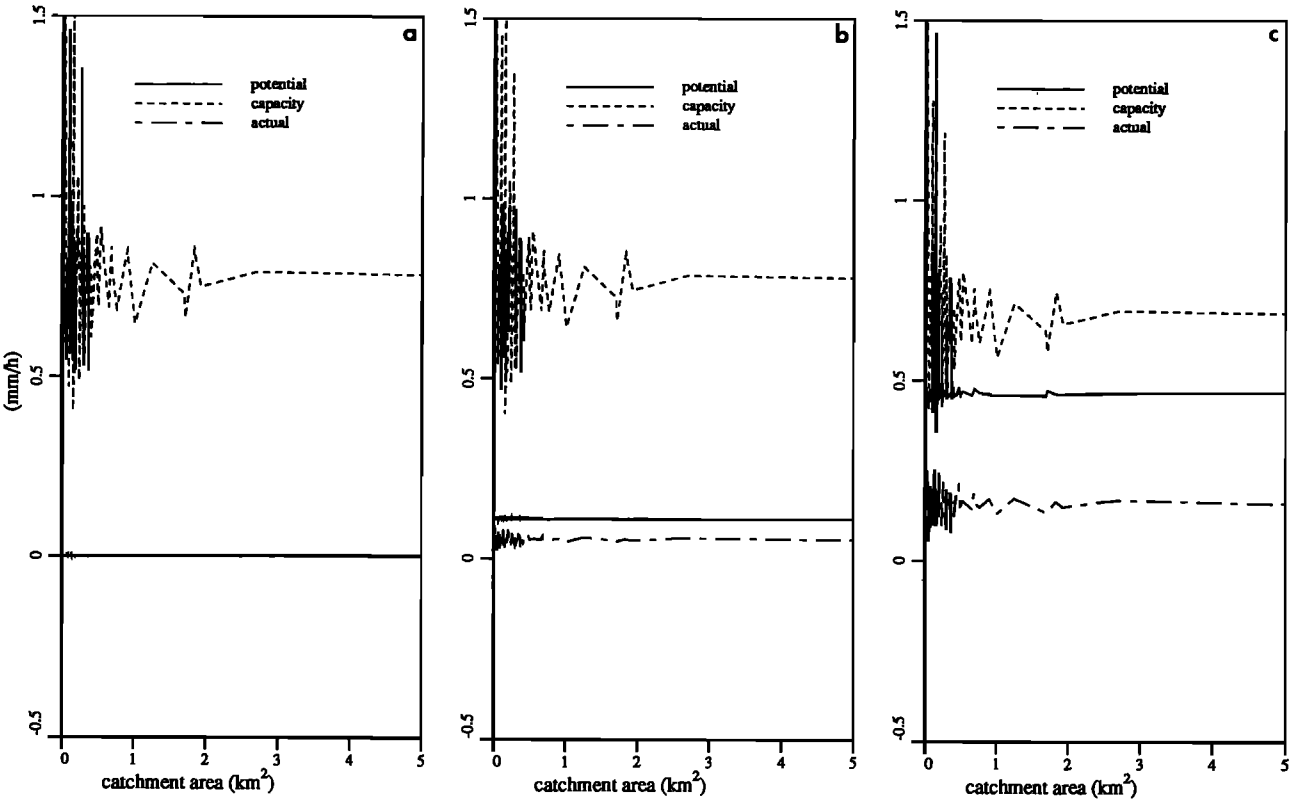

Figure 9. Computed catchment-average potential evaporation, exfiltration capacity (soil-controlled evaporation), and actual evaporation versus catchment area for October 7, 1987: (a) 1245, (b) 1415, and (c) 1815 UT.

Evapotranspiration

Famiglietti and Wood [1994a] compute the local rate of evapotranspiration, $e(i)$, as

$$e(i) = f_{bs}(i)e_{bs}(i) + f_v(i)[e_{wc}(i) + e_{dc}(i)] \quad (2)$$

where f_{bs} is the local fraction of bare soil, f_v is the local fraction of vegetated soil, e_{wc} is rate of evaporation from the wet canopy, and e_{dc} is rate of transpiration from the dry canopy. The catchment-average evapotranspiration rate is simply the average of the local rates, or the sum of the average bare-soil, wet canopy, and dry canopy components of evapotranspiration.

Figure 11 shows the catchment-average evapotranspiration rate versus catchment scale at 1415 UT, October 7, 1987. The catchment-average bare-soil, dry canopy, and wet canopy evaporation components are plotted as well. The weighted sum of these components yields the catchment-average evapotranspiration rate at any scale. The variability in the catchment-average evapotranspiration rate with scale is therefore a function of the variability of its components.

The catchment-average evapotranspiration rate versus catchment scale is shown in Figure 4a for 1245, 1415, and 1815 UT, October 7, 1987. The scaling behavior of catchment-average evapotranspiration reflects that of its components, described in detail above for bare-soil evaporation. The variability at small scales increases with time until midday. The REA scale shows a corresponding increase with time, from small scales in the morning, to 1.0–2.0 km^2 at midday. Both the increased variability at small scales and the increase in the REA scale reflect the change in the dominant controls on the catchment-average evapotranspiration rate, from those associated with potential rates in the morning, to those associated with soil- and vegetation-controlled rates at midday.

Discussion

Effects of Spatial Variability and Scale on Areally Averaged Evapotranspiration

The previous sections have shown that for the simulations conducted in this study, the dominant controls on the scaling behavior of catchment-average evapotranspiration depend on the dominant controls on its components: evaporation from the wet canopy, transpiration from the dry canopy, and evaporation from bare soils. The controls on these components depend, in turn, on whether evapotranspiration is occurring at potential rates or soil- and vegetation-controlled rates.

In general, when root zone moisture content levels are relatively high or the potential evapotranspiration rates are low, evapotranspiration will occur at predominantly potential rates. The scaling behavior of catchment-average evapotranspiration under these conditions is largely determined by the controls on the potential evapotranspiration rates. When root zone moisture content levels are low or potential evapotranspiration rates are high, evapotranspiration will occur at soil- and vegetation-controlled rates. The scaling behavior of catchment-average evapotranspiration is then dominated by the controls on the soil- and vegetation-controlled rates.

This interaction between the land surface and the atmosphere will have both seasonal and diurnal timescales. For

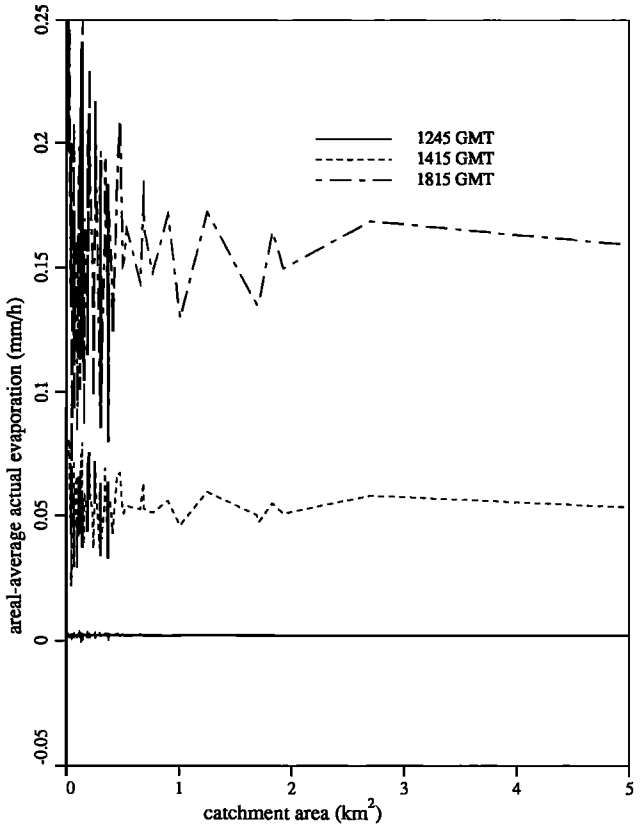

Figure 10. Computed catchment-average actual evaporation rate versus catchment area for 1245, 1415, and 1815 UT, October 7, 1987.

example, during wetter periods, evapotranspiration will occur at predominantly potential rates. However, the space-time variability in atmospheric forcing and moisture content, as well as the spatial variability in vegetation and soils, will result in portions of the catchment evaporating at soil- or vegetation-controlled rates if the potential evapotranspiration rate is too high (e.g., at midday), or if moisture content levels fall too low (e.g., during an extended interstorm period). Conversely, during dry periods, more evapotranspiration will occur at moisture-stressed rates, but some or all of the catchment may evaporate at potential rates when the potential rates are low (e.g., in the early morning) or if root zone moisture contents rise to high levels (e.g., after a storm). The seasonal and diurnal dynamics of land-atmosphere interaction will therefore be reflected in the scaling behavior of catchment-average evapotranspiration.

Implications for Hydrologic Modeling

This study investigates the importance of spatial variability in land surface and atmospheric variables for modeling evapotranspiration at the catchment scale. The existence of an REA for simulated evapotranspiration provides insight into how spatial variability in critical variables such as soil moisture, topography, and vegetation can be incorporated into hydrological models. At scales greater than the REA scale, much of the variability in the underlying distributions of land surface parameters and atmospheric forcing has been sampled. At these scales, a statistical representation of spatial variability in important model parameters and inputs may be adequate for evapotranspiration modeling (i.e., a statistically aggregated model of land hydrologic processes may be an appropriate representation for catchment evapotranspiration modeling). At scales less than the REA scale, explicit patterns of important spatially variable model parameters and inputs may have a significant impact on simulated evapotranspiration. At these scales a spatially explicit aggregation approach may be required to model catchment-average evapotranspiration.

One example of a statistical aggregation procedure is given by *Famiglietti and Wood* [1994a]. They present a statistical-dynamical macroscale hydrological model, in which a local water and energy balance model is aggregated with respect to a probability density function of the combined topographic-soil index. (Note that the local model is the same as that incorporated in the spatially distributed model used in this study. See the appendix for a description of the macroscale model.) The spatial variability in topographic and soil properties results in spatial variability in modeled moisture content and the water and energy fluxes related to moisture content, such as runoff and evapotranspiration. All other model parameters and inputs in the statistical model are represented by catchment-average values in accordance with the concept of local hydrologic similarity. However, when spatial variability in these other parameters is correlated to the spatial distribution of the topographic-soil index (e.g., vegetation parameters), it can easily be incorporated into the model framework.

Figure 12 compares catchment-average evapotranspiration

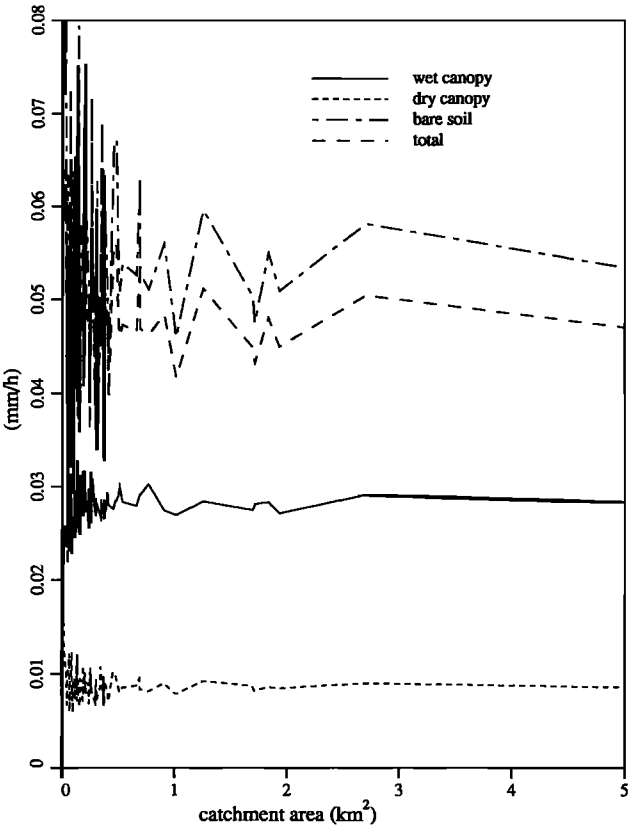

Figure 11. Computed catchment-average evapotranspiration rate, catchment-average wet canopy evaporation rate, catchment-average dry canopy transpiration rate, and catchment-average bare-soil evaporation rate versus catchment area for 1415 UT, October 7, 1987.

computed for the King's Creek catchment (for October 5–9, 1987) using the spatially distributed model, the statistically aggregated macroscale model, and the one-dimensional local model (in which all model inputs and parameters are held at catchment-average values). Note that this effective parameter approach is commonly employed in land surface parameterizations within atmospheric models at their grid scale or subgrid scale (O(100 km) or O(10 km), respectively).

The solid line in Figure 12 represents the control simulation of evapotranspiration computed using the spatially distributed model with all model inputs and parameters varying spatially. The short-dashed line represents evapotranspiration computed with the statistically aggregated model. The difference between the two simulations results from the combined effect of representing spatially variable moisture content statistically and all other model inputs and parameters with catchment-average values (e.g., solar radiation, vegetation, soil properties). The dot-dashed line represents evapotranspiration computed with the one-dimensional model. The one-dimensional simulation represents the effect of holding all model inputs and parameters, including initial root zone moisture content and the topographic-soil index, at catchment-average values. At the catchment scale there is little difference between spatially distributed and statistically aggregated simulations at the King's Creek catchment. However, there is a significant difference between the simulations run with spatially constant and spatially variable initial root zone moisture content.

Figure 12 clearly indicates that at the King's Creek catchment during IFC4, a period when soil and vegetation controls of evapotranspiration were active and thus nonlinearly related to soil moisture, modeled evapotranspiration does not scale up during midday hours. Obviously, under such conditions an effective parameter approach is invalid. The considerable bias between evapotranspiration computed with spatially variable root zone moisture content and catchment-average moisture content indicates further that some representation of spatial variability in root zone moisture content (and in this case the topographic-soil index) more so than other model parameters, is required for realistic simulation of evapotranspiration during this time period. Figure 12 also shows that at the scale of the King's Creek catchment, which is greater than the REA scale, a statistical representation of spatial variability in topographic-soil index, and thus root zone moisture content, is an adequate representation of the actual patterns represented within the spatially distributed model. Finally, the minimal difference between evapotranspiration computed with the spatially distributed and statistical macroscale model shows that at the King's Creek catchment, the concept of local hydrologic similarity (i.e., that topographic and soil properties dominate downslope moisture redistribution and thus hydrologic response) seems reasonable for interstorm processes modeled during IFC4 at this location. (Note that *Famiglietti and Wood* [1994b] attribute this result to a lack of spatial variability in other catchment characteristics such as soil and vegetation properties and meteorological forcing. However, *Famiglietti and Wood* [1994a, b] review a modeling approach to deal with the possible breakdown of the concept in the presence of greater variability and at larger spatial scales.)

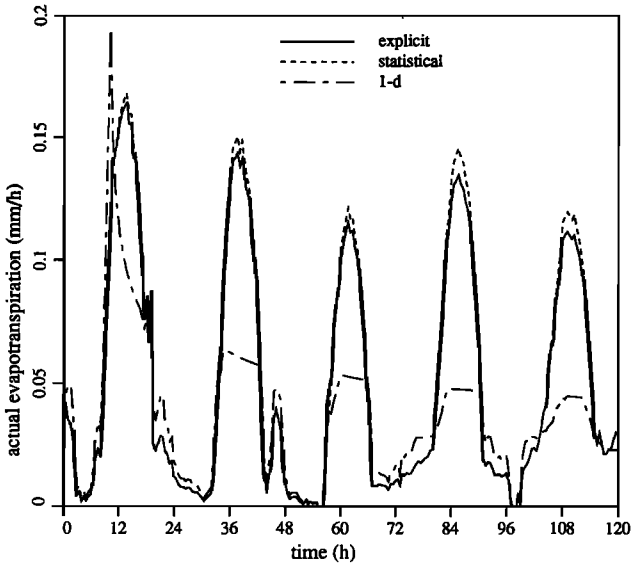

Figure 12. Computed catchment-average evapotranspiration using the spatially distributed model (explicit), the statistically aggregated model (statistical), and the one-dimensional local model (1-d), October 5–9, 1987.

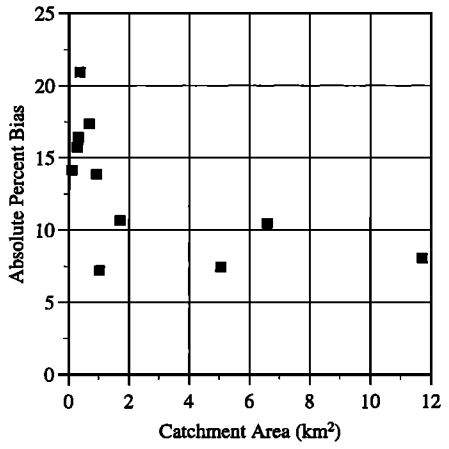

Figure 13. Comparison of catchment-average evapotranspiration rates computed with the spatially distributed model (control run) and the statistically aggregated model, for several of the subwatersheds shown in Figure 2. Results shown as absolute percent bias (see text) versus subcatchment area, and are averaged in time over October 5–7, 1987.

To investigate the importance of explicit spatial patterns in determining areally averaged evapotranspiration rates at scales smaller than the REA scale, the statistical model was run for 11 of the small subwatersheds shown in Figure 1 on the western side of the King's Creek catchment. Areally averaged evapotranspiration rates were computed for the first three days of IFC4 and compared with those rates computed in the control run with the spatially distributed model. For each simulation time step, the percent bias was computed as the absolute difference between control run and statistical model evapotranspiration rates, normalized by the control run rate. These results were averaged for the simulation for each subwatershed, and plotted in Figure 13 versus catchment area. Figure 13 shows that for the subwatersheds with areas less than 2 km^2, the statistical and control simulations differ by 7–21%. As subcatchment area increases, the difference between the two simulations varies over a smaller range, from 7% to 11%. This figure offers evidence that the statistical model can perform poorly at smaller scales, or conversely, that explicit spatial

patterns may play a significant role in determining areally averaged evapotranspiration in the small subwatersheds of the King's Creek catchment.

As previously mentioned, we chose to simulate evapotranspiration during IFC4 at the King's Creek catchment in order to investigate the role of spatial variability in root zone moisture content. Consequently, these results may be in part site, model, and time dependent. For example, a site with greater spatial variability in vegetation may show a stronger dependence on vegetation parameters than root zone soil moisture content. In that case, evapotranspiration models for areas larger than the REA might include a distribution function representing the spatial pattern of vegetation rather than moisture content. Or, if the comparison shown in Figure 12 were repeated during IFC3 (August 6–21, 1987), a period during which root zone moisture content was relatively wet and evapotranspiration occurred at potential rates, then spatial variability in moisture content may not be the dominant control on the scaling behavior of areally averaged evapotranspiration. Under these land and atmospheric conditions, evapotranspiration may scale up more readily. Similarly, we suggest that later in the year or, in general, when the spatial distribution of root zone moisture content is relatively dry with little spatial variability, even though evapotranspiration may occur under active soil and vegetation control, it may again scale up readily.

However, we believe that the findings presented here provide a framework for understanding and modeling areally averaged evapotranspiration at the catchment and larger scales. The existence of an REA for both evapotranspiration and storm runoff response suggests that the problem of continuous water and energy balance modeling at the catchment scale can be greatly simplified. As shown above, in areas larger than the REA, spatial patterns of dominant process controls can be represented by their statistical distribution functions. These results may also have implications for hydrological modeling at the larger spatial scales associated with atmospheric modeling. Since the length scale of the REA is much smaller than the length scale of atmospheric model grid cells, the existence of an REA for both storm and interstorm process modeling offers encouragement that important subgrid-scale land surface heterogeneity can be represented rather simply within model grids (or their subgrid patches) by means of statistical distribution functions.

Finally, the concept that the dominant controls on areally averaged evapotranspiration vary with the amount of land surface evaporating at potential rates versus soil or vegetation-controlled rates is, we propose, site independent and applicable at larger scales. At these larger scales (O(100 km)) the variability in the various components of areally averaged evapotranspiration may be a function of large-scale controls that are not evident at the catchment scale. For example, topographic, soil, and vegetation properties may vary on the scale of regional geology and climate. Soil moisture may vary on the scale of storm systems. Potential evapotranspiration may vary with synoptic-scale weather patterns and variations in vegetation and soil properties. The behavior of areally averaged evapotranspiration from the catchment scale to the scale of a GCM grid, and the land surface-atmosphere conditions under which evapotranspiration will scale up, are the subjects of ongoing research.

Summary

In this paper we explored the effect of spatial variability and scale on areally averaged evapotranspiration. We employed a spatially distributed model to determine the effect of explicit patterns of model parameters and atmospheric forcing on modeled areally averaged evapotranspiration over a range of increasing spatial scales, from the local scale to the catchment scale. The study catchment was the King's Creek catchment, an 11.7 km^2 watershed located on the native tallgrass prairie of Kansas.

This paper shows that an REA exists for catchment-scale evapotranspiration modeling at the King's Creek catchment. The size of the REA was shown to vary diurnally, reaching a maximum of 1–2 km^2 by midday. The dominant controls on the scaling behavior of catchment-average evapotranspiration, and thus the size of the REA, were shown to depend on the dominant controls on its components: evaporation from the wet canopy, transpiration from the dry canopy, and evaporation from bare soils. The controls on these components depend, in turn, on whether evapotranspiration is occurring at potential rates or soil- and vegetation-controlled rates. During FIFE IFC4, a period when soil and vegetation controls of evapotranspiration were active and thus nonlinearly related to soil moisture, spatial variability in root zone moisture content was shown to be the dominant control on areally averaged evapotranspiration for the catchment.

The existence of an REA for evapotranspiration modeling suggests that in catchment areas smaller than the REA, actual patterns of model parameters and inputs (e.g., root zone moisture content, soil properties, vegetation, solar radiation) may be important factors governing catchment-scale evapotranspiration rates. In models applied at scales greater than the REA scale, spatial patterns of dominant process controls can be represented by their statistical distribution functions. This point was demonstrated at the King's Creek catchment, where as mentioned above, the spatial distribution of root zone moisture content was shown to be a dominant process control. Simulations of catchment-scale evapotranspiration showed that at this scale, which was greater than the REA scale, a statistical representation of the spatial pattern of soil moisture yielded minimally biased results compared with fully spatially distributed simulations.

The existence of an REA for both evapotranspiration and storm runoff response suggests that the problem of continuous water and energy balance modeling at the catchment scale can be greatly simplified, in that spatial patterns of important process controls can be represented by their statistical distribution functions. Their existence may also have implications for hydrological modeling at the larger spatial scales associated with atmospheric modeling. Since the length scale of the REA is much smaller than the length scale of atmospheric model grid cells, the existence of an REA for both storm and interstorm process modeling offers encouragement that important subgrid-scale land surface heterogeneity can be represented rather simply within model grids (or their subgrid patches) by means of statistical distribution functions.

Although this work was performed for a specific location at the catchment scale, we believe that some of the concepts outlined here are fairly general. Therefore we believe that these findings will provide a framework for understanding the scaling behavior of areally averaged evapotranspiration at the catchment and larger scales.

Appendix: Model Descriptions

Spatially Distributed Water and Energy Balance Model

In this section, the spatially distributed water and energy balance model of *Famiglietti and Wood* [1994a] is briefly de-

scribed. The catchment is discretized into a number of grid elements, and digital topographic, vegetation, soil, and other model parametric information and inputs are coregistered to the model grid. Local hydrologic fluxes are modeled at each grid element of the catchment using the simple soil-vegetation-atmosphere transfer scheme (SVATS), also described in detail by *Famiglietti and Wood* [1994a]. Explicit spatial variability is incorporated into the model by allowing all model parameters, inputs, and outputs to vary between grid elements. Catchment grid elements are coupled in the subsurface using simple, topographically based expressions for lateral saturated flow. The catchment-scale hydrologic fluxes are the average of the individual grid-element fluxes.

At the surface of each grid element, the SVATS recognizes bare soil and vegetated land cover. Vegetation is further partitioned into wet and dry canopy. The soil column between the land surface and the water table is partitioned into a near-surface root zone and a deeper transmission or percolation zone. The local water table depth is the lower boundary condition for the local model.

A land surface energy balance is computed for each model grid element to determine the potential evaporation for bare soil, unstressed transpiration for the dry canopy, and evaporation from the wet canopy. The canopy water balance is used to calculate the net precipitation. These variables, in conjunction with precipitation on bare soils, constitute the atmospheric forcing in the model.

The equations for vertical transport of soil moisture include infiltration into bare and vegetated soils, evaporation from bare soils, transpiration by vegetation, capillary rise from the water table, drainage from the root zone and transmission zone, and runoff from bare and vegetated soils. Each of these vertical moisture fluxes depends on the soil moisture status of the local root zone or the transmission zone, and the local soil properties. The infiltration, evapotranspiration, and surface runoff fluxes also depend on local rates of atmospheric forcing. Canopy and soil water balance equations are applied at each grid element in the catchment to monitor the states of wetness in the local canopy, root zone, and transmission zone.

Saturated subsurface flow between catchment grid elements is assumed controlled by the spatial variability in topographic and soil properties. The local topographic-soil index of *Beven* [1986] is employed to parameterize this variation between catchment grid elements. *Sivapalan et al.* [1987] derived a simple expression for the local water table depth z in terms of the local topographic-soils index, $\ln \{(aT_e)/(T \tan \beta)\}$:

$$z = z_{\text{ave}} - (1/f)[\ln \{(aT_e)/(T \tan \beta)\} - \lambda] \qquad \text{(A1)}$$

where z_{ave} is the catchment-average water table depth, f is a parameter that describes the exponential decay of saturated hydraulic conductivity with depth, a is the area drained through the local unit contour, T_e is the catchment average value of the saturated transmissivity coefficient (saturated hydraulic conductivity divided by f), T is the local value of the transmissivity coefficient, β is the local slope angle, and λ is the catchment-average value of the topographic variable $\ln (a/\tan \beta)$. The areal average water table depth is updated by consideration of catchment-scale mass balance.

The catchment-scale evapotranspiration E is given by

$$E = (1/N) \sum_{i \in C} \{f_{\text{bs}}(i)e_{\text{bs}}(i) + f_v(i)[e_{\text{dc}}(i) + e_{\text{wc}}(i)]\} \qquad \text{(A2)}$$

Table A1. Catchment-Averaged Model Parameters

Parameter	Description	Value
	Soil	
K_s, mm/h	saturated hydraulic conductivity	6.34
θ_S	saturation moisture content	0.47
θ_r	residual moisture content	0.04
ψ_c, m	air entry suction head	0.30
B	pore size distribution index	0.16
D, m	damping depth of surface temperature	0.50
α	bare-soil albedo	0.15
z_0, m	bare-soil roughness length	0.001
z_{rz}, m	root zone depth	0.50
	Vegetation	
α	wet canopy albedo	0.25
α	dry canopy albedo	0.20
z_0	canopy roughness length	0.09
d, m	canopy zero-plane displacement	0.37
r_{stmin}, s/m	minimum stomatal resistance	110.0
ψ_{crit}, m	critical leaf water potential	−210.0
F	root activity factor	10^4
L, m/m	root density	2.0
R_u, s/m	root resistance	9.77×10^9
LAI	leaf area index	0.37
f_v	areal fraction of vegetation	0.39
	Topography	
λ	catchment-average topograpic-soil index	3.74

where N is the number of grid elements in the catchment, C is the set of all grid elements in the catchment, all other terms have been previously defined.

The catchment-scale runoff flux Q is the average of local bare-soil and vegetated runoff components. A lateral subsurface flow component Q_b is also included in the catchment-scale flux. The grid-scale runoff is expressed as

$$Q = (1/N) \sum_{i \in C} [f_{\text{bs}}(i)q_{\text{bs}}(i) + f_v(i)q_v(i)] + (Q_b/A) \qquad \text{(A3)}$$

where q_{bs} is the runoff from bare-soil land surface, q_v is the runoff from vegetated land surface, and A is the catchment surface area.

The model is driven with time series of standard meteorological inputs, including precipitation, shortwave radiation, longwave radiation, wind speed, air temperature, humidity, and pressure and can accommodate spatial patterns of each. The model also requires spatial patterns of soil, vegetation, and the topographic-soil index. A description of model parameters and their average values for the King's Creek catchment are given in Table A1.

Statistically Aggregated Macroscale Water and Energy Balance Model

A statistical distribution of the topographic-soil index forms the framework of this TOPMODEL-based water and energy balance model known as TOPLATS (TOPMODEL-based land-atmosphere transfer scheme). The distribution of the index is discretized into a number of intervals, and the local SVATS described above is applied at each interval. Equation (A1) provides the lower boundary condition (the local water table depth) for each interval of the distribution, effectively coupling intervals together through the process of saturated lateral subsurface flow. The areally averaged hydrologic fluxes are the weighted average of the local fluxes, where the local weighting function is the probability of occurrence of the par-

ticular interval, e.g., areally averaged evapotranspiration is computed as

$$E = \sum_{i \in D} \{f_{bs}(i)e_{bs}(i) + f_v(i)[e_{dc}(i) + e_{wc}(i)]\}p(i) \qquad \text{(A4)}$$

where i now represents a particular interval of the discretized topographic-soil index distribution, $p(i)$ its probability of occurrence, and D is the distribution of the index. The statistical model requires areally averaged meteorological inputs (described above) and soil and vegetation parameters in addition to the distribution of the topographic-soil index. See Table A1 for the average values of these parameters for the King's Creek catchment used in this study.

Acknowledgments. This work was supported by NASA grants NAGW-1392 and NGT-60153; this research support is gratefully acknowledged. This paper was revised while the first author visited both Princeton University and the National Center for Atmospheric Research under the sponsorship of the UCAR Climate System Modeling Program (CSMP). The use of facilities at those institutions and the support of CSMP is greatly appreciated. We thank Ralph Dubayah for providing spatially distributed solar radiation data for the FIFE site. We thank Dominique Thongs for providing the spatial averaging software and for his help in processing other spatially distributed FIFE data. This work benefited greatly from discussions with David Wolock and the comments of two anonymous reviewers. Page charges for this paper were paid by the Geology Foundation of the Department of Geological Sciences at the University of Texas at Austin.

References

Beven, K., Runoff production and flood frequency in catchments of order n: An alternative approach, in *Scale Problems in Hydrology*, edited by V. K. Gupta, I. Rodriguez–Iturbe, and E. F. Wood, pp. 107–131, D. Reidel, Norwell, Mass., 1986.

Bloschl, G., R. B. Grayson, and M. Sivapalan, On the representative elementary area (REA) concept and its utility for distributed rainfall-runoff modeling, *Hydrol. Process.*, in press, 1995a.

Bloschl, G., D. Gutknecht, R. B. Grayson, and M. Sivapalan, Organisation, randomness and scale in hydrologic modelling, *Hydrol. Process.*, in press, 1995b.

Dooge, J. C. I., Looking for hydrologic laws, *Water Resour. Res.*, *22*(9), suppl. 46S–58S, 1986.

Famiglietti, J. S., Aggregation and scaling of spatially-variable hydrological processes: Local, catchment-scale, and macroscale models of water and energy balance, Ph.D. dissertation, Dep. of Civ. Eng. and Oper. Res., Princeton Univ., Princeton, N. J., 1992.

Famiglietti, J. S., and E. F. Wood, Multiscale modeling of spatially variable water and energy balance processes, *Water Resour. Res.*, *30*(11), 3061–3078, 1994a.

Famiglietti, J. S., and E. F. Wood, Application of multiscale water and energy balance models on a tallgrass prairie, *Water Resour. Res.*, *30*(11), 3079–3093, 1994b.

Holwill, C. J., and J. B. Stewart, Spatial variability of evaporation derived from aircraft and ground-based data, *J. Geophys. Res.*, *97*(D17), 18,623–18,628, 1992.

Jedlovec, G. J., and R. J. Atkinson, Variability of geophysical parameters from aircraft radiance measurements for FIFE, *J. Geophys. Res.*, *97*(D17), 18,913–18,924, 1992.

Schimel, D. S., T. G. F. Kittel, A. K. Knapp, T. R. Seastedt, W. J. Parton, and V. B. Brown, Physiological interactions along resource gradients in a tallgrass prairie, *Ecology*, *72*(2), 672–684, 1991.

Schmugge, T. J., J. R. Wang, and G. Asrar, Results from the push broom microwave radiometer flights over the Konza Prairie in 1985, *IEEE Trans. Geosci. Remote Sens.*, *26*(5), 590–596, 1988.

Sellers, P. J., F. G. Hall, G. Asrar, D. E. Strebel, and R. E. Murphy, An overview of the First International Satellite Land Surface Climatology Project (ISLSCP) Field Experiment (FIFE), *J. Geophys. Res.*, *97*(D17), 18,345–18,371, 1992.

Sivapalan, M., K. J. Beven, and E. F. Wood, On hydrologic similarity, 2, A scaled model of storm runoff production, *Water Resour. Res.*, *23*(12), 2266–2278, 1987.

Sivapalan, M., E. F. Wood, and K. J. Beven, On hydrologic similarity, 3, A dimensionless flood frequency model using a generalized geomorphologic unit hydrograph and partial area runoff generation, *Water Resour. Res.*, *26*(1), 43–58, 1990.

Wood, E. F., and C. Hebson, On hydrologic similarity, 1, Derivation of the dimensionless flood frequency curve, *Water Resour. Res.*, *22*(11), 1549–1554, 1986.

Wood, E. F., M. Sivapalan, K. J. Beven, and L. Band, Effects of spatial variability and scale with implications to hydrologic modeling, *J. Hydrol.*, *102*, 29–47, 1988.

Wood, E. F., M. Sivapalan, and K. J. Beven, Similarity and scale in catchment storm response, *Rev. Geophys.*, *28*(1), 1–18, 1990.

Woods, R., and M. Sivapalan, Investigating the representative elementary area: An approach based on field data, *Hydrol. Process.*, in press, 1995.

J. S. Famiglietti, Department of Geological Sciences, University of Texas at Austin, Austin, TX 78712. (e-mail: jfamiglt@maestro.geo.utexas.edu)

E. F. Wood, Water Resources Program, Department of Civil Engineering and Operations Research, Princeton University, Princeton, NJ 08544.

(Received February 9, 1994; revised October 27, 1994;
accepted October 28, 1994.)